Spatial Multi-Omics Identifies a NOTCH3-Mediated Capillary–mCAF Crosstalk Driving Immune Exclusion in Hepatocellular Carcinoma

Fansen Ji[1,2#], Haochen Li[3#], Qi Wang[1#], Jiawei Zhang[4], Ying Xiao[5], Huan Li[5], Hao Liu[5], Tanqing Long[6], Boyang Wu[1], Hao Chen[1], Haoming Xia[1], Xinquan Liu[7, 8], Chuanrui Xu[6], Yibo Gao[7, 8], Bingjun Tang[1,*], Juan Liu[1,*], Shizhong Yang[1,*], Jiahong Dong[1,*]

[1] Hepatopancreatobiliary Center, Beijing Tsinghua Changgung Hospital, Key Laboratory of Digital Intelligence Hepatology (Ministry of Education), School of Clinical Medicine, Tsinghua Medicine, Tsinghua University, 102218, Beijing, China.
[2] Tsinghua-Peking Center for Life Sciences. 100084, Beijing, China.
[3] School of Medicine, Tsinghua Medicine, Tsinghua University, 100084, Beijing, China.
[4] Health Management Center, Beijing Jishuitan Hospital, Capital Medical University, 100035, Beijing, China.
[5] Department of Pathology, Beijing Tsinghua Changgung Hospital, Tsinghua University, 102218, Beijing, China.
[6] School of Pharmacy, Tongji Medical College, Huazhong University of Science and Technology, 430030, Wuhan, Hubei, China.
[7] Department of Thoracic Surgery, National Cancer Center/National Clinical Research Center for Cancer/Cancer Hospital, Chinese Academy of Medical Sciences and Peking Union Medical College, Beijing, 100021, China.
[8] Central Laboratory & Shenzhen Key Laboratory of Epigenetics and Precision Medicine for Cancers, National Cancer Center/National Clinical Research Center for Cancer/Cancer Hospital & Shenzhen Hospital, Chinese Academy of Medical Sciences and Peking Union Medical College, 518116, Shenzhen, China.

Fansen Ji, Haochen Li, Qi Wang, Xiaojuan Wang, Jiawei Zhang, Ying Xiao, Huan Li, et al. 2026. Spatial Multi-Omics Identifies a NOTCH3-Mediated Capillary–mCAF Crosstalk Driving Immune Exclusion in Hepatocellular Carcinoma. ***iMeta*** 5: e70117.
https://doi.org/10.1002/imt2.70117

Background: Fibrosis and disease progression

Several organs are prone to fibrosis

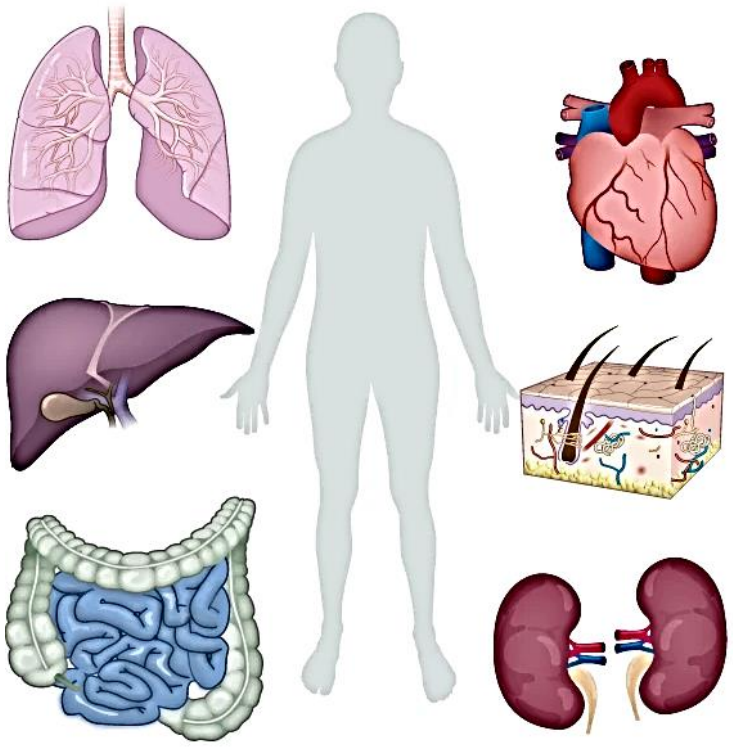

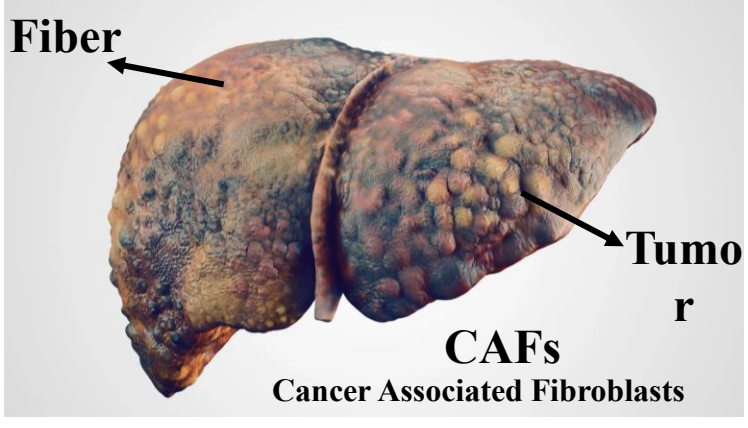

The primary mechanism of liver fibrosis

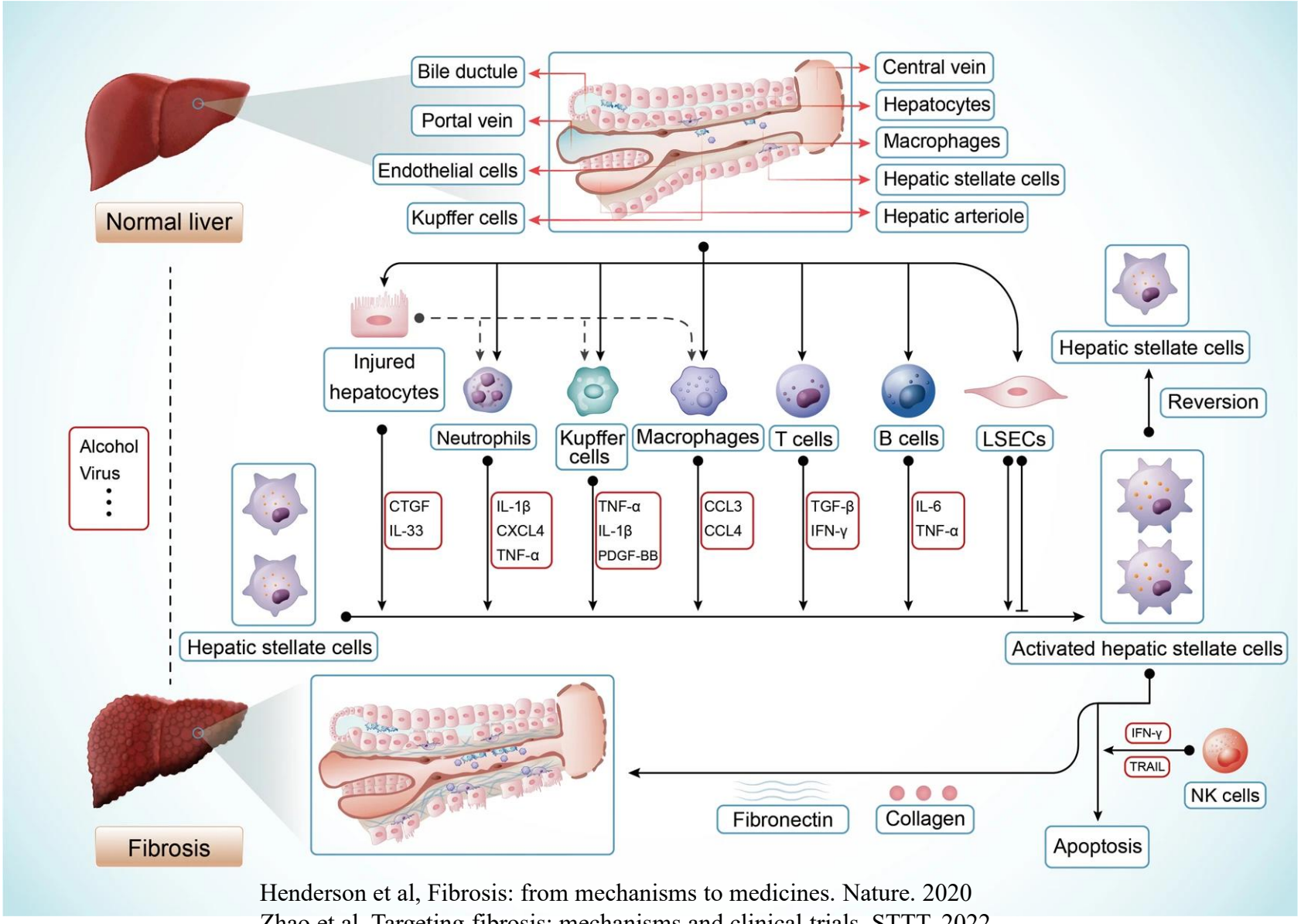

Henderson et al, Fibrosis: from mechanisms to medicines. Nature. 2020
Zhao et al, Targeting fibrosis: mechanisms and clinical trials. STTT. 2022.

Background: CAFs - heterogeneity in function and distribution

Matrix CAFs - mCAFs

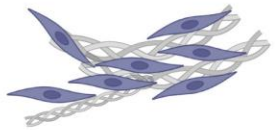

MMP11, POSTN, *CTHRC1*, LRRC15, FAP

COL11A1, PDPN, *MMP14*, COL1A1, VIM, SMA/*ACTA2*, S100A4, *Dcn*, *Lum*/*LUM*, *Vcan*, *Col14a1*, *Fbln1*, *Fbln2*, *Smoc*, *Lox*, *Loxl1*, *Cxcl14*, *COL6A3*, *FN1*, *COL3A1*, *SPON2*, *COL5A1*, PDGFRA, *INHBA*

Tumor-like CAFs - tCAFs

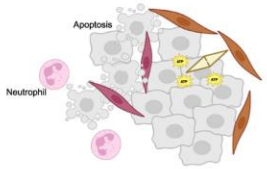

CD73/*NT5E*, CD10/*MME*, FAP

PDPN, *NDRG1*, *GPR77*, *Slc2a1*, *TSPAN8*

Vessel-associated CAFs - vCAFs

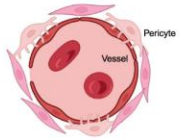

CD146/*MCAM*, SMA/*ACTA2*, NOTCH3, COL18A1

NOTCH3, *COL18A1*, *Nr2f2*, *VEGF*

Dividing CAFs - dCAF

Cell division, Ki-67/*MKI67*

TUBA1B

Inflammatory CAFs - iCAFs

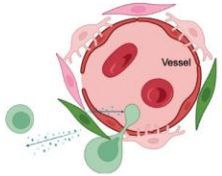

IL6, *IL1*, CD34, *PLA2G2A*, *DPP4*, *CFD*, *C3*, *Pi16*

Il6, *Il1*, *CXCL12*, *CXCL14*, SMA/*ACTA2*, *CXLC1*, *HGF*, *CXCL2*, PDGFRA, FAP, VIM, *IGF1*, *CXCL13*, *ALDH1A1*, *CCL19*, CCL21, *IL8*, *CCL2*, *C4b*, *PTGSDS*, *S100A4*, *DES*

Interferon response CAFs – ifnCAFs

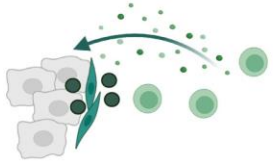

CXCL9, *CXCL10*, *CXCL11*, IDO/*IDO1*

SLC14A1, *NRG1*, *BMP5*, *STC1*, *Cxcl9*, *Cxcl10*, *Cxcl11*, *IL32*

Reticular-like CAFs - rCAFs

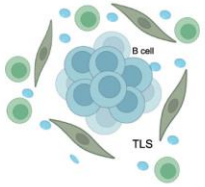

CCL19, CCL21

CFD, *CXCL14*, *MMP14*, *ADH1B*, *CXCL12*, *IL6*, *NOTCH3*, *PDGFA*, *VCAM1*, *CXCL13*, *CCL5*

Antigen-presenting CAFs - apCAFs

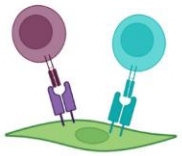

HLA-DR, *HLA-DQ*, CD74

IGFBP3, *CXCL12*, *RBP1*, *HLA-DPB1*, *COLEC11*, *TMEM56*, *CCL2*

Cords et al, Classifying cancer-associated fibroblasts—The good, the bad, and the target. Cancer Cell. 2024.

Highlights

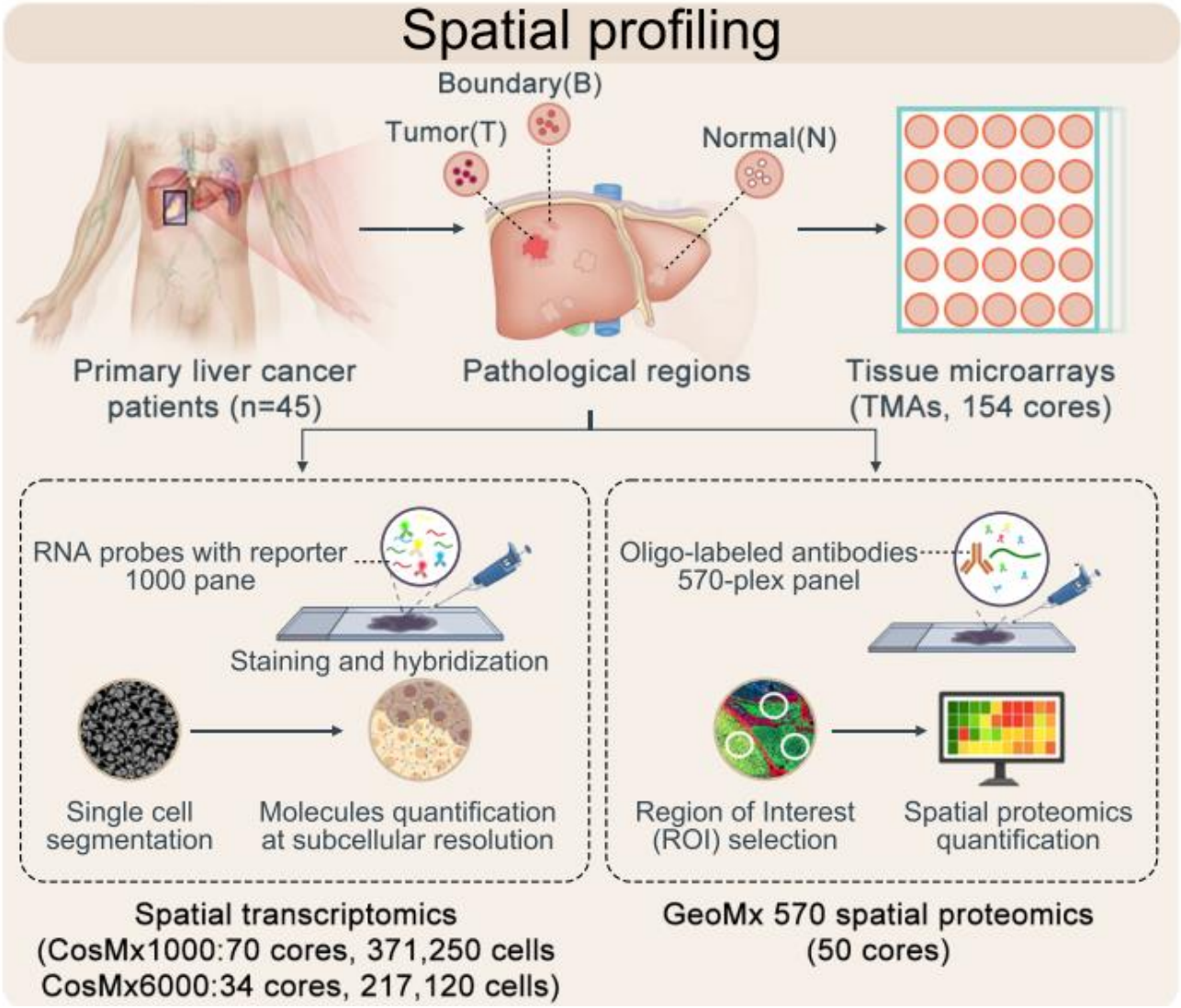

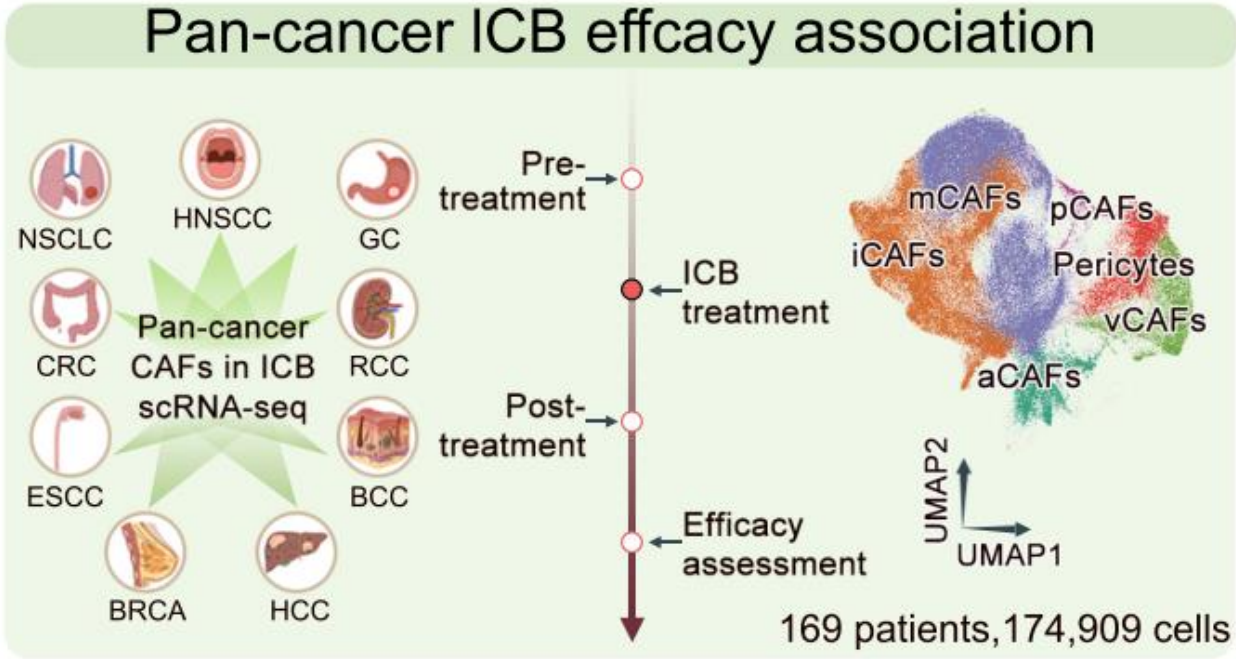

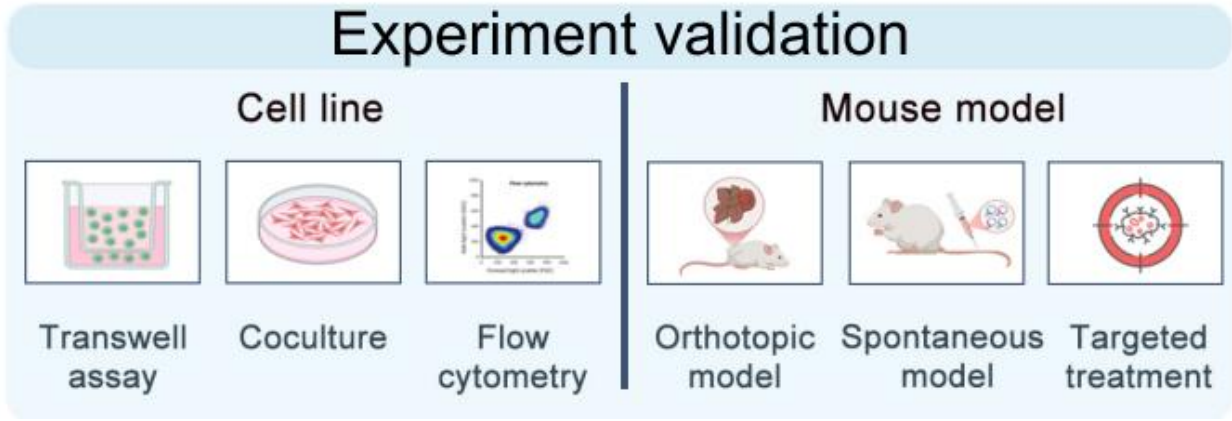

- Building a spatial high-res multi-omics atlas of HCC reveals DLL4-NOTCH3-driven capillary-mCAF axis sculpts fibrotic, immune-excluded tumors.
- Integrating pan-cancer scRNA-seq & spatial data shows mCAF collagen polarization drives ICB resistance.
- NOTCH3 inhibition reduces fibrosis, boosts T cell infiltration, and synergizes with anti-PD-1, offering a translable HCC therapy.

Single-cell spatial transcriptomic profiles reveal coordinated cellular topography in HCC

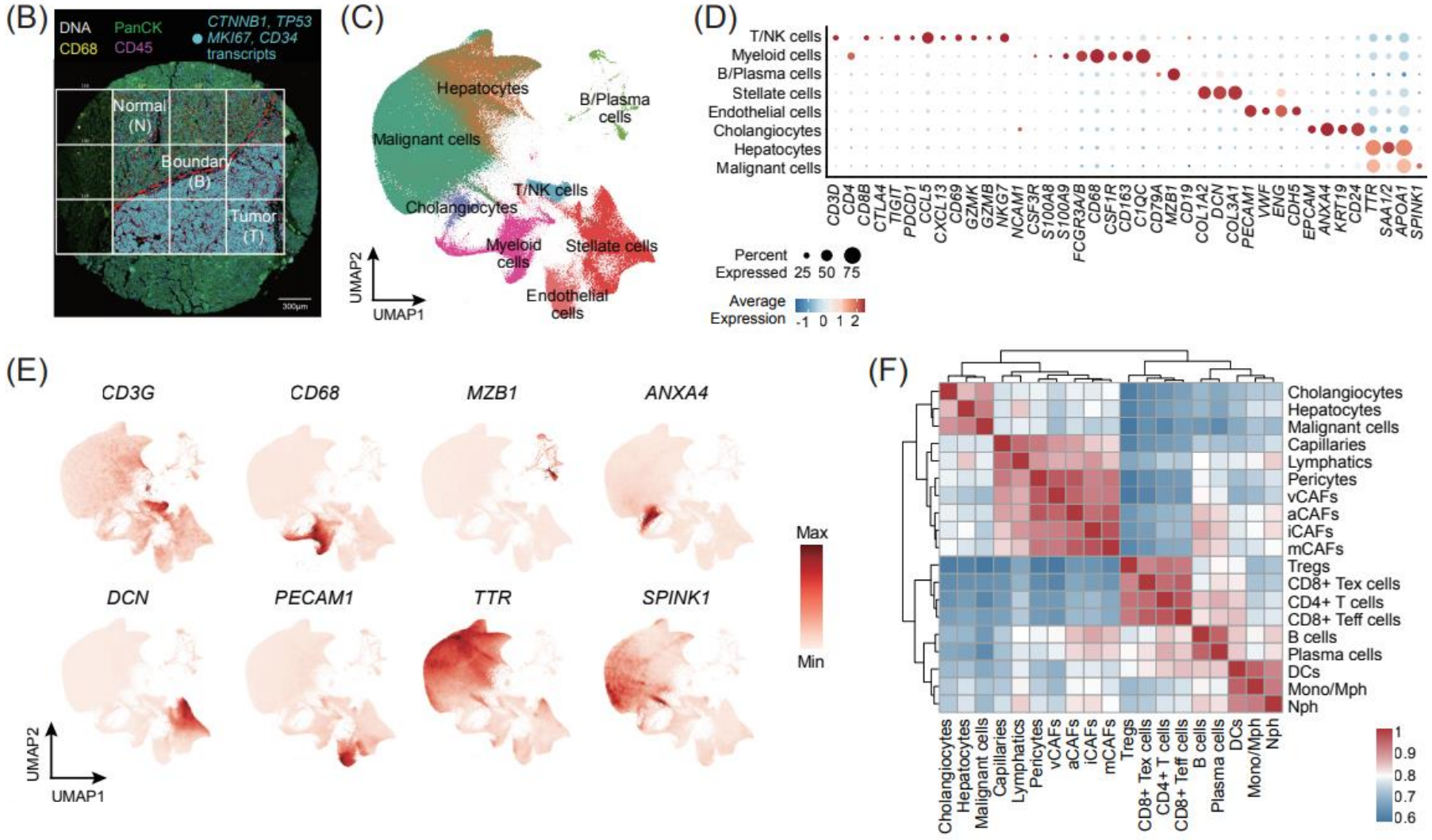

(B) Representative immunofluorescence image of a tissue microarray core, showing Tumor (T), Boundary (B), and Normal (N) regions overlaid all transcripts of *CTNNB1*, *MKI67*, *TP53* and *CD34* to each Field of View (FOV), in which invasive boundary has been outlined. (C) UMAP visualization of all cells in CosMx1000 data, colored by annotated cell lineages, including Malignant cells, Hepatocytes, Cholangiocytes, Myeloid cells, Stellate cells, Endothelial cells and B/Plasma cells. (D) Dot plot showing the expression of canonical marker genes across major lineages. (E) Gene expression profiles of canonical marker genes across major cell types from CosMx1000 cohort. (F) Gene expression correlation matrix between cell types from CosMx1000 cohort.

CosMx SMI precisely matches HE, IF, and spatial transcriptomics

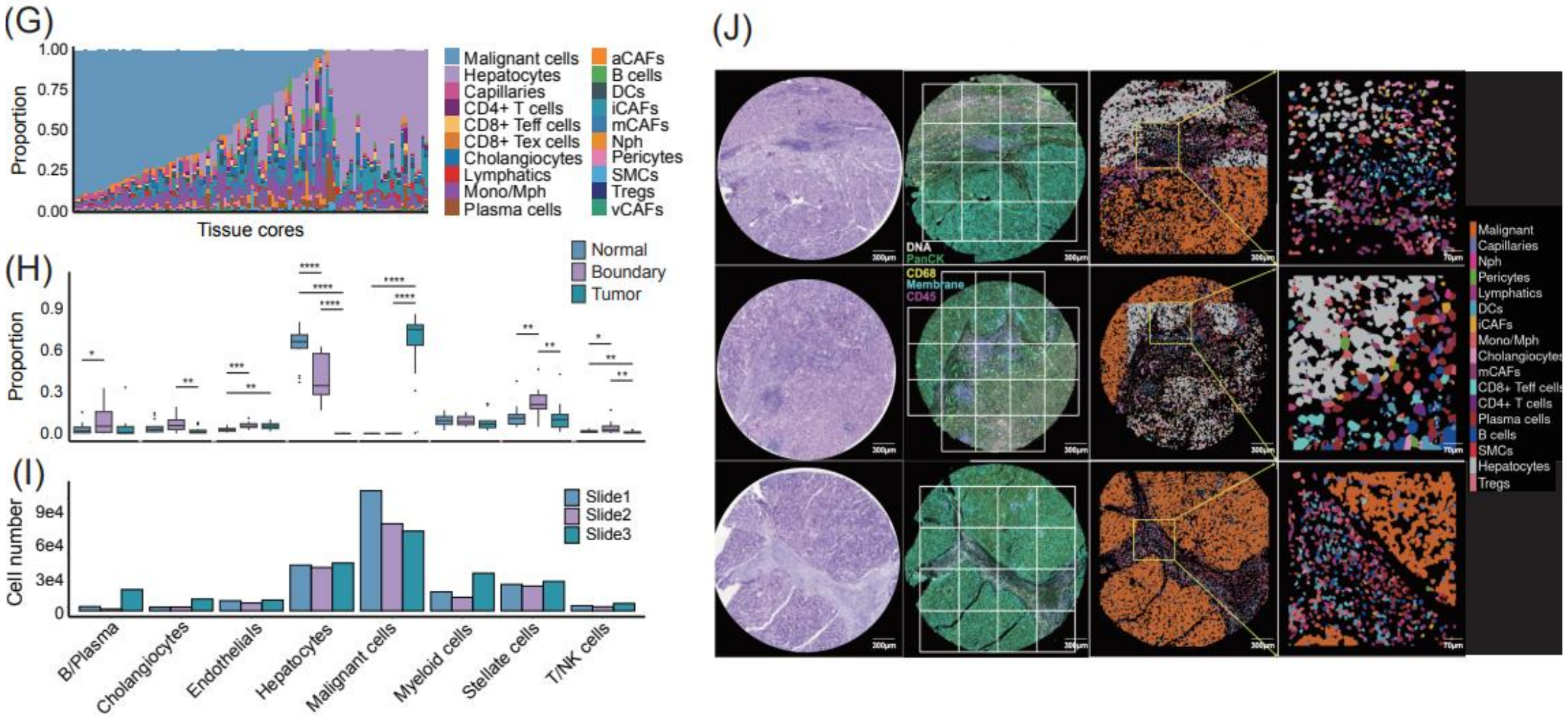

(G) Relative proportions of major cell types across all tissue cores. (H) Comparison of cell type proportions among Tumor, Boundary, and Normal regions. The x-coordinate represents each lineage, consistent with the x-axis in (I)**.** (I) Comparison of cell type components among different spatial transcriptomics profiling slides (Slide 1, 2: CosMx1000; Slide 3: CosMx6000). (J) Representative spatial maps of cell types overlaid with H&E and immunofluorescence (IF) staining from selected tissue cores, illustrating the spatial organization of the tumor microenvironment.

Spatial data reveal tumor cell expression heterogeneity

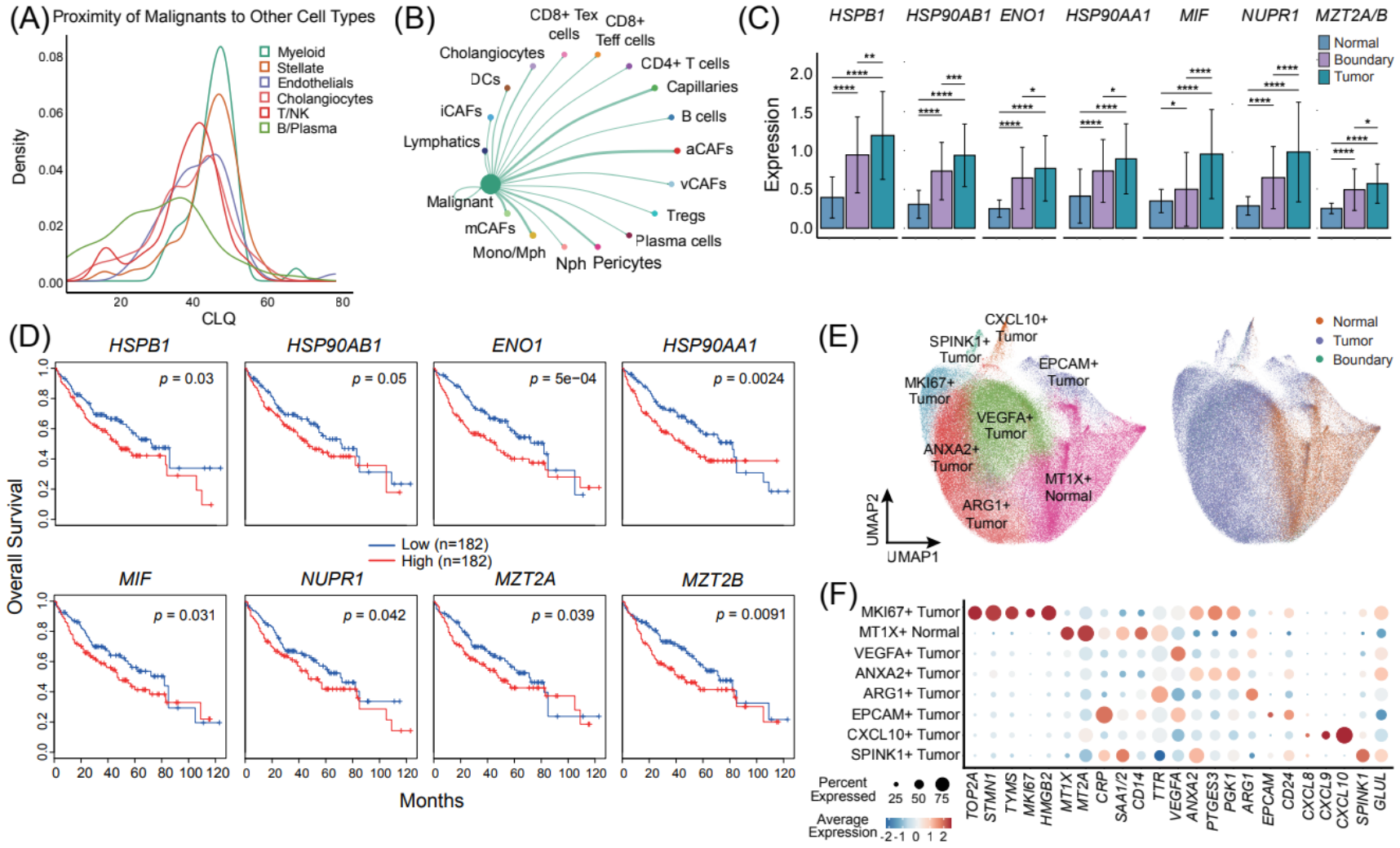

(A) Density of Colocalization Quotient, illustrating the spatial proximity of malignant cells to other lineages. CLQ, a metric measuring the ratio of observed to expected spatial co-occurrence, where rightward-shifted peaks indicate a higher frequency of strong colocalization (**Methods**). (B) Cell-cell communication network analysis of malignant cells to other cell types in CosMx1000 dataset. The analysis incorporated spatial constraints, restricting inferred interactions to biologically feasible distances based on defined interaction ranges for diffusible molecules and contact ranges for contact-dependent signaling. The thickness of the connecting lines represents the interaction strength (communication probability), calculated based on the expression levels of ligand-receptor pairs. (C) Expression levels of key oncogenic and stress response genes (*HSPB1, HSP90AB1, HSP90AA1, ENO1, MIF, NUPR1, MZT2A/B*) across Normal, Boundary and Tumor. (D) Kaplan-Meier survival curves for patients with high (red line) and low expression levels (blue line) of key oncogenic and stress response genes. (E) UMAP visualization of all hepatocyte subtypes (including malignant and normal hepatocytes, left) and corresponding Normal, Boundary and Tumor regions (right). (F) Dot plot showing the expression of canonical marker genes across hepatocyte subtypes.

mCAF niches negatively correlate with patient prognosis

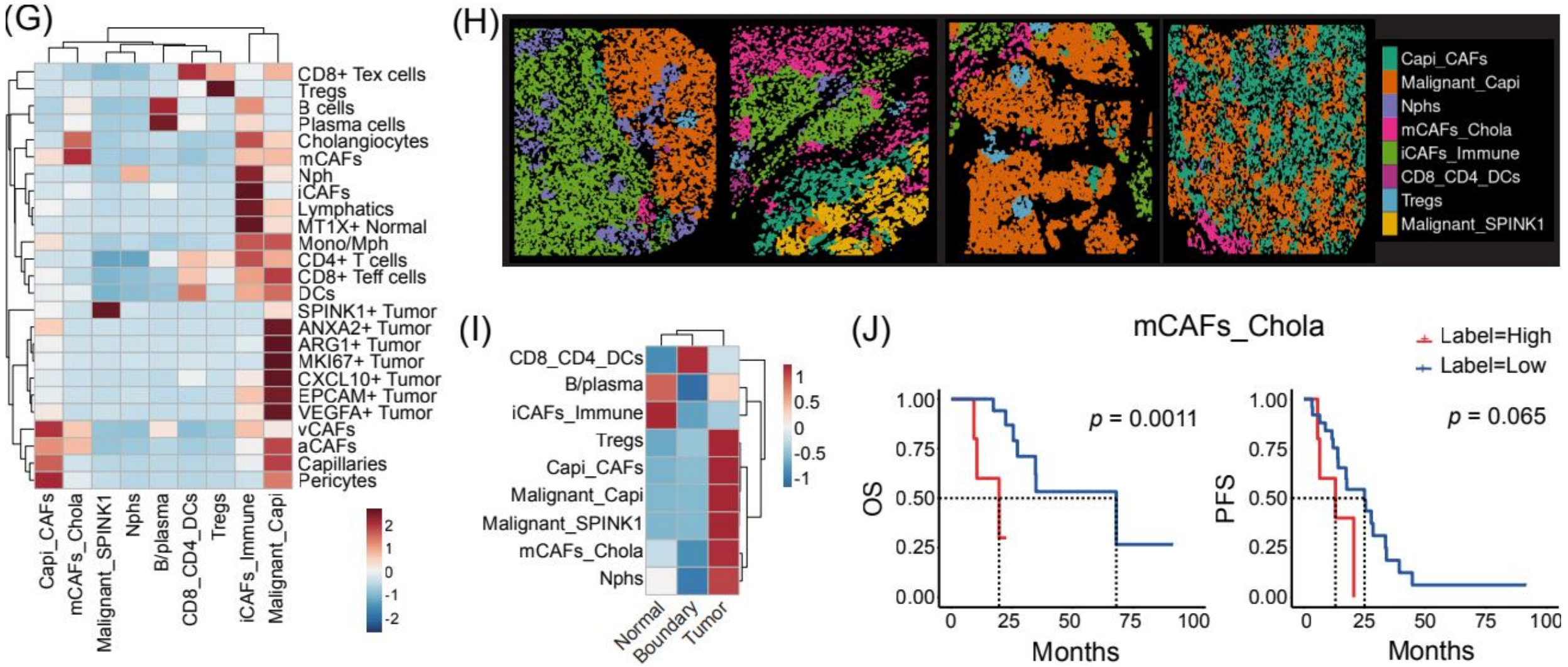

(G) Heatmap of normalized cell type component enrichment in each identified spatial niche. (H) Representative spatial image plot of identified spatial niches. (I) Heatmap of normalized spatial niche component enrichment in each tissue region (Normal, Boundary, and Tumor). (J) Kaplan-Meier survival curves for patients with high and low abundance of mCAFs_Chola niche, indicating significant association with poor OS and PFS.

Cancer associated fibroblasts exhibit functional and spatial heterogeneity

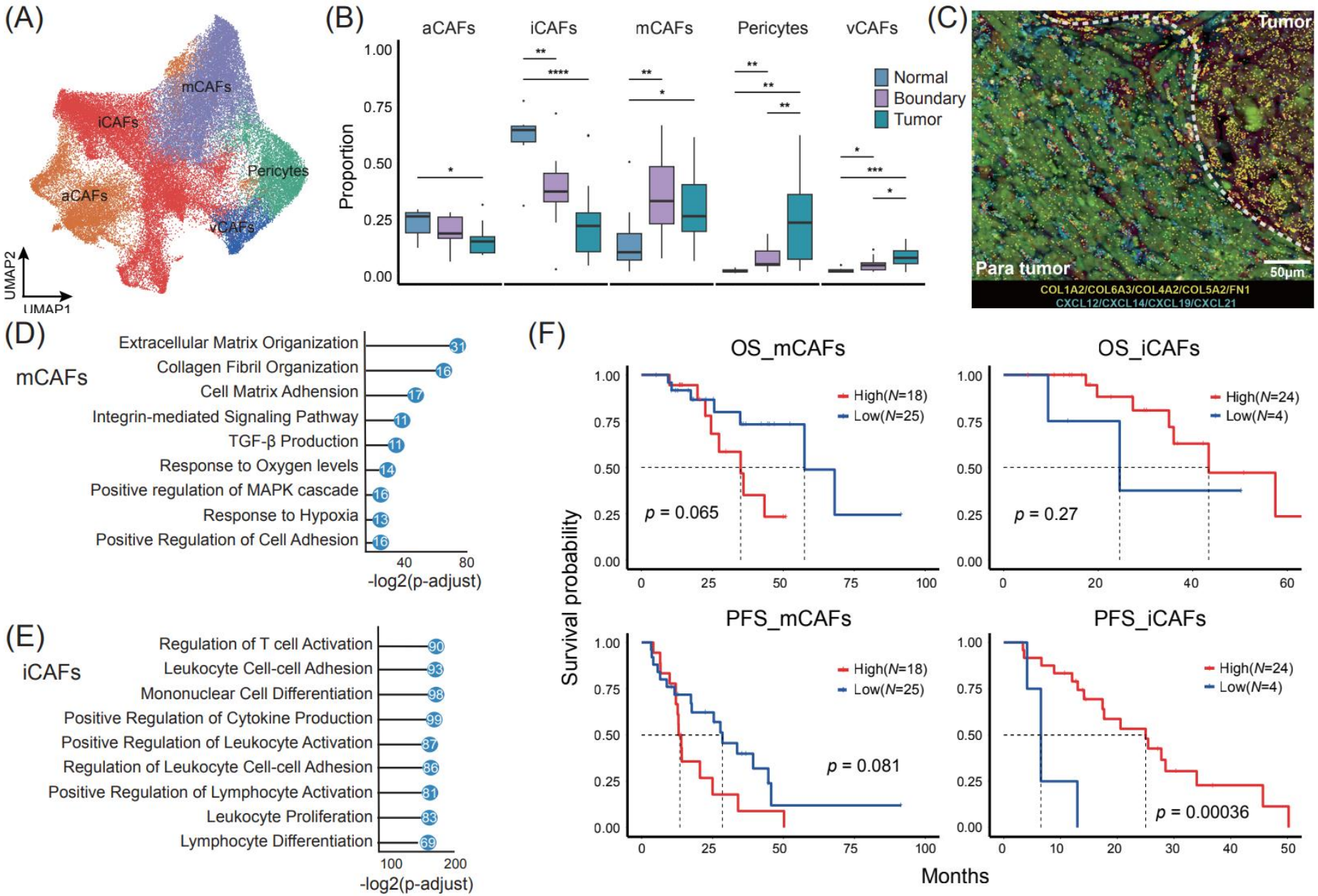

(A) Identification of five distinct CAF subpopulations in spatial data: mCAFs, iCAFs, antigen-presenting CAFs (aCAFs), vascular CAFs (vCAFs) and pericytes. (B) Proportion of different CAF subtypes across Normal, Boundary, and Tumoral regions. (C) Spatial distribution of mCAF and iCAF markers across Normal, Boundary, and Tumor regions overlaid in IF image, where mCAF associated marker genes are labeled in yellow, iCAF associated marker genes are labeled in Cyan, and invasive boundary was outlined in White. (D) Gene Ontology (GO) enrichment analysis highlighting functional pathways in mCAFs. (E) GO enrichment analysis highlighting functional pathways in iCAFs. (F) Kaplan-Meier survival curves showing the prognostic significance of mCAF and iCAF proportion. High mCAF infiltration is associated with worse overall survival (OS) and progression-free survival (PFS).

iCAFs and mCAFs serve as prognostic indicators

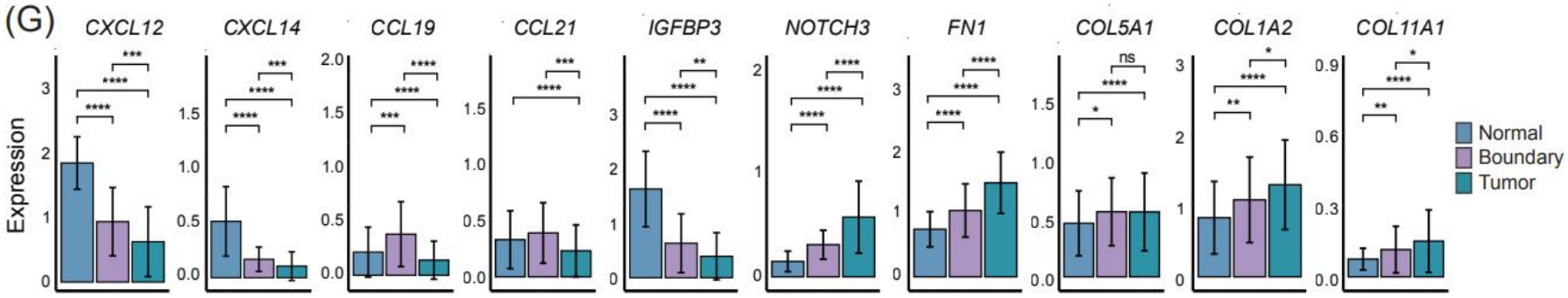

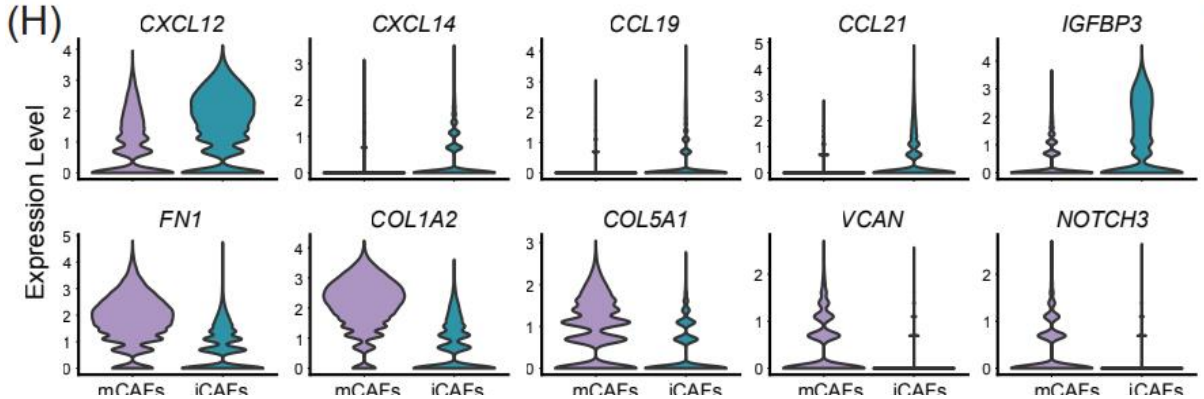

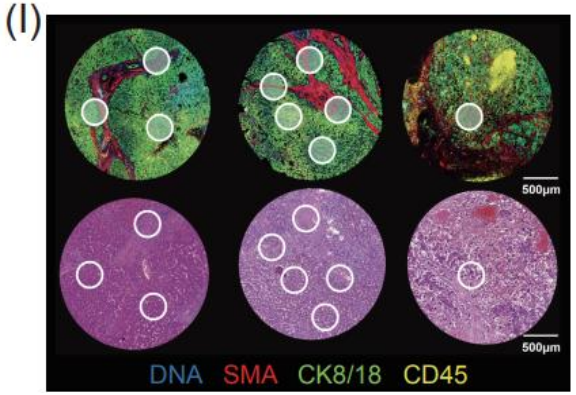

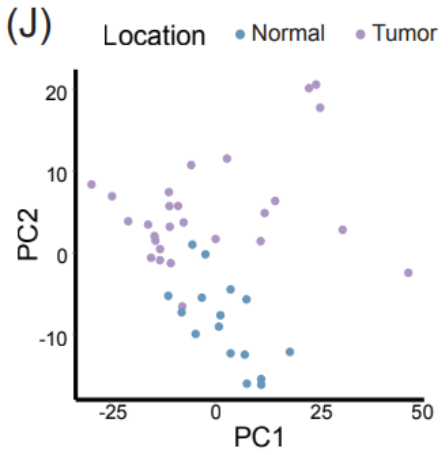

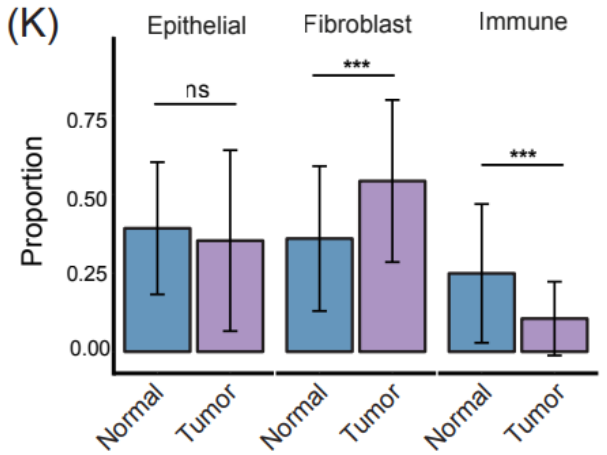

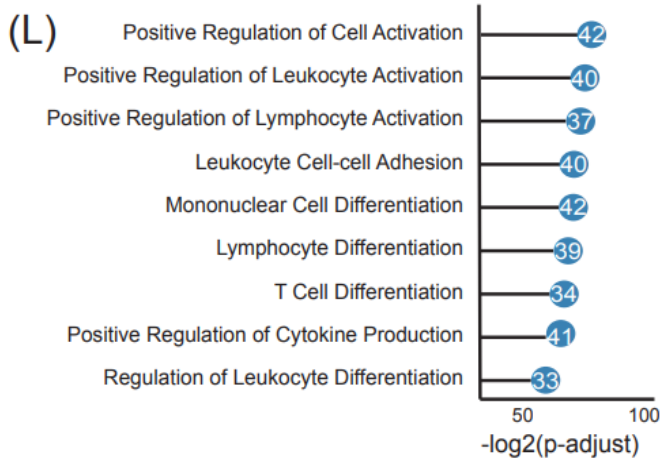

(G) Expression of iCAF-associated genes (*CXCL12*, *CXCL14*, *CCL19*, *CCL21*) and mCAF-associated genes (*FN1, COL1A2, COL11A1, COL5A1, NOTCH3*) in CAFs across Normal, Boundary and Tumoral regions. (H) Violin plot showing the expression of marker genes between iCAFs and mCAFs. (I) Paired IF and H&E images showing the spatial proteomic profiling on FFPE specimens from HCC patients using the GeoMx Immune-Oncology Protein Panel. A total of 95 regions of interest (ROIs) were selected to represent Tumor, Boundary and Normal tissues. (J) Principal component analysis (PCA) reveals a clear segregation of proteomic profiles between Tumor and Normal regions. (K) Quantitative cell-type proportion of Epithelial, Fibroblast and Immune compartment across Tumor and Normal regions. (L) Gene Ontology (GO) enrichment analysis of differentially expressed proteins of ROIs from Normal regions in GeoMx spatial proteomics data.

mCAF polarization correlates with ICB response

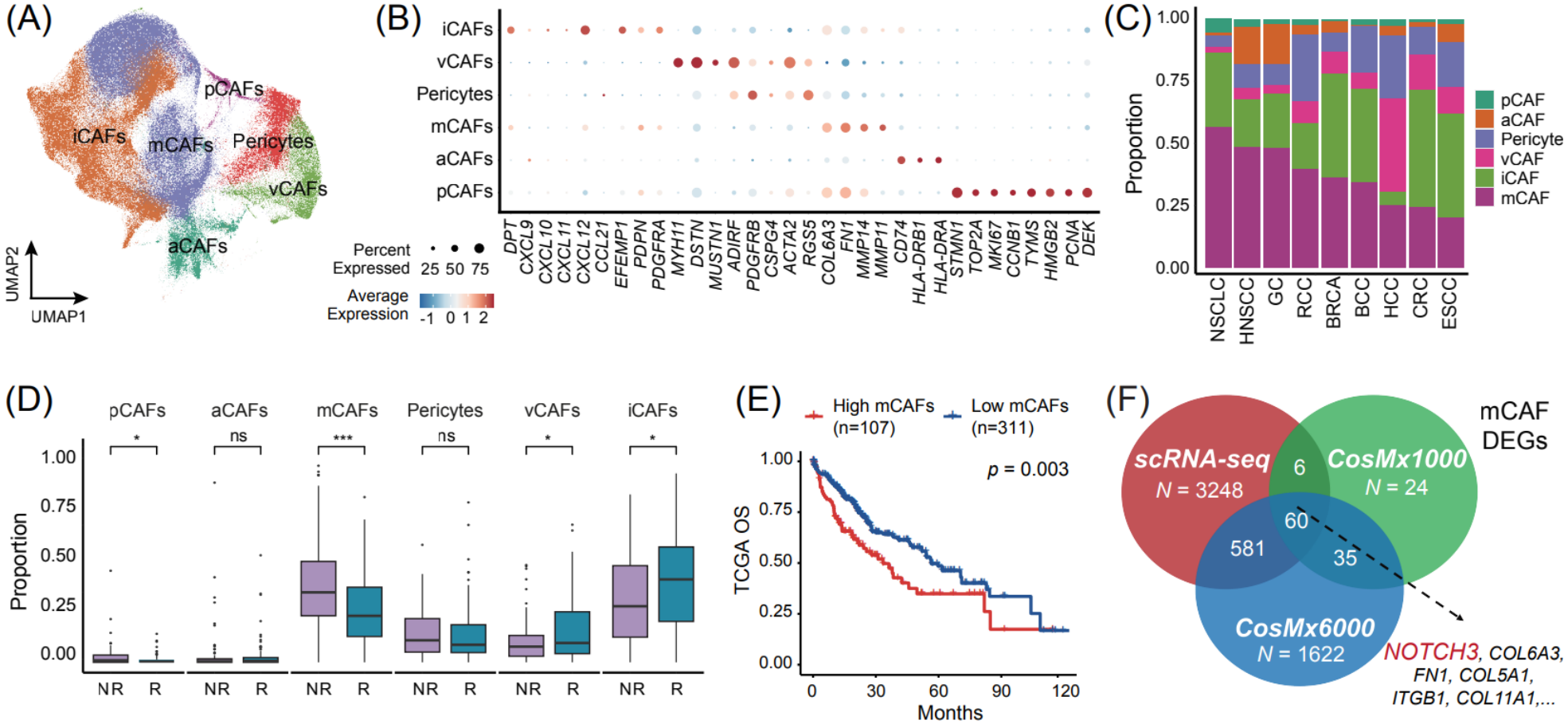

(A) UMAP plot showing the clustering of different CAF subtypes in pan-cancer scRNA-seq data under ICB treatment. (B) Dot plot representing the average expression levels of select marker genes for each CAF subtype. (C) Stacked bar plots showing the distribution of CAF subtypes across various cancer types. (D) Box plots showing the proportion of each CAF subtype in non-responders (NR) and responders (R) under ICB treatment. (E) Kaplan-Meier survival curves showing the association between mCAF proportion and clinical outcomes (OS) in TCGA-LIHC data. (F) Venn diagram showing the overlap of mCAF differentially expressed genes (DEGs) from scRNA-seq and two spatial transcriptomic datasets (CosMx1000 and CosMx6000). The intersection (n=60) is constrained by the CosMx1000 panel size (~1000 genes) but represents 48% (60/125) of the total mCAF DEGs identified in this dataset. *NOTCH3* consistently identified as a robust marker of mCAFs.

Capillary-mCAF crosstalks via the DLL4-NOTCH3 axis

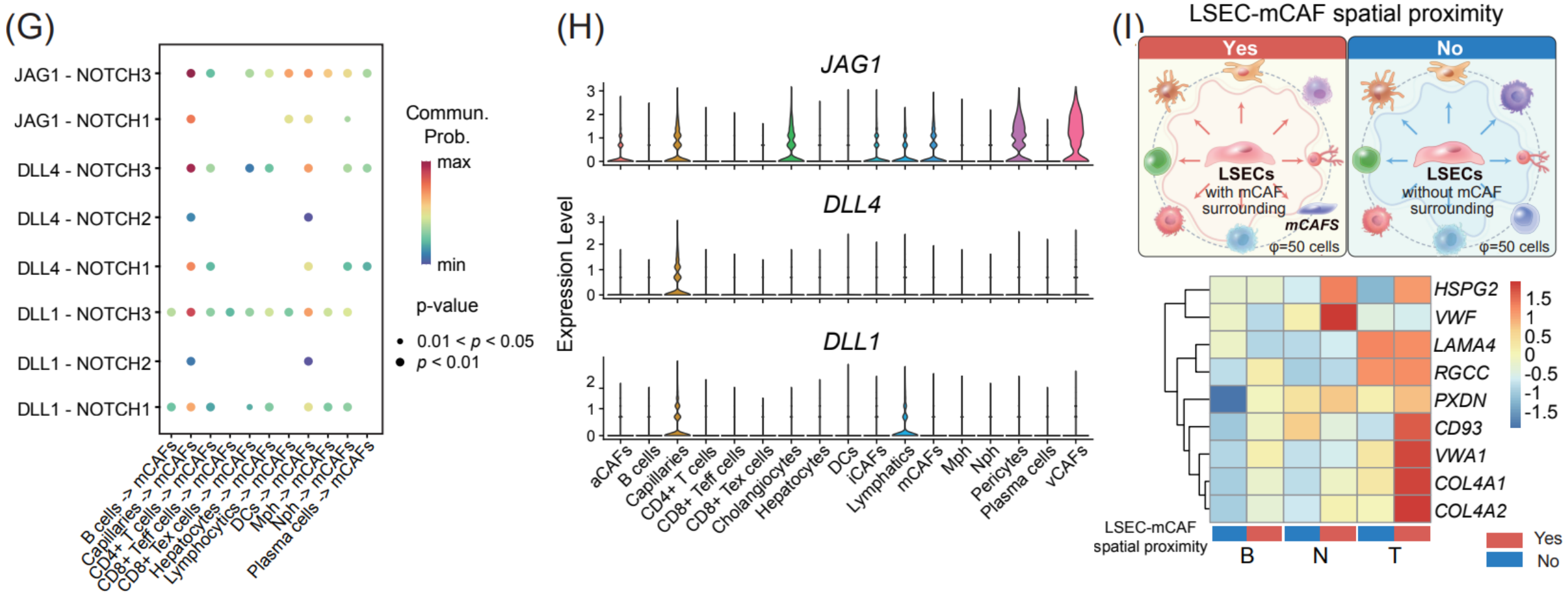

(G) CellChat ligand-receptor interaction analysis revealing significant cross talk of the NOTCH signaling pathway between capillaries and mCAFs in CosMx1000 data, primarily mediated by *DLL4/NOTCH3, JAG1/NOTCH3*, and *DLL1/NOTCH3* interactions. (H) Expression levels of *DLL1*, *DLL4*, and *JAG1* across different cell types, showing the sources of these ligands. (I) Schematic diagram for determining whether there is spatial proximity of mCAFs to each liver sinusoidal endothelial cell (LSEC) within 50 spatial neighbors. The below one is Heatmap showing the expression levels of angiogenesis-related genes in LSECs with (Yes, red) or without (No, blue) spatial proximity to mCAFs.

Capillary-derived DLL4 triggers mCAF polarization

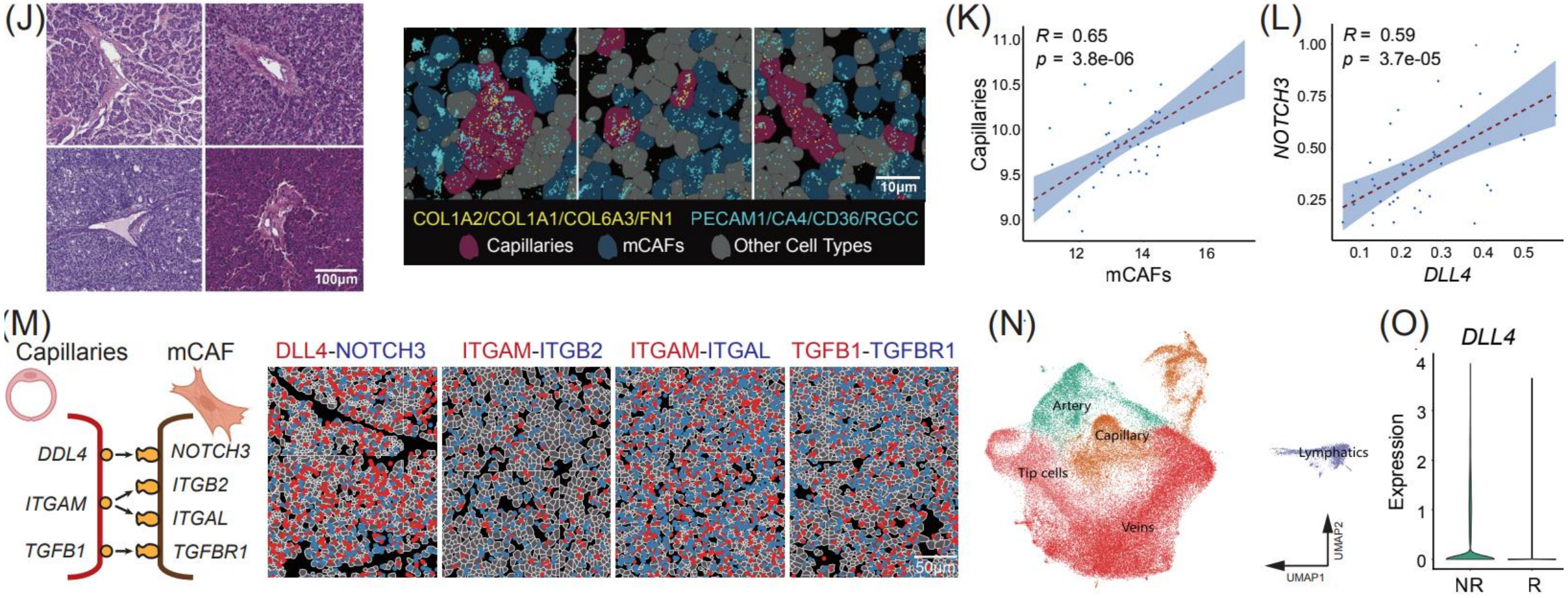

(J) H&E staining and CosMx spatial images illustrated the spatial proximity between capillaries and mCAFs. The H&E image provides histopathological context at the tissue level from an independent cohort, while the IF/ISH panels are representative images illustrating the spatial co-localization patterns of capillaries and mCAFs identified from the CosMx spatial transcriptomic analysis. (K) Dot plot showing the spatial correlation between mCAF and capillary signatures for each ROI in GeoMx spatial proteomic data. (L) CosMx data revealing the correlation between *DLL4* and *NOTCH3* expression for each FOV. (M) CosMx Spatial imaging data illustrating capillaries-mCAF interactions mediated by different ligands and receptors. (N) UMAP visualization of pan-cancer endothelial subtypes under ICB treatment. (O) Comparing *DLL4* expression between ICB non-responders (NR) and responders (R) for capillaries.

NOTCH3-driven collagen polarization promotes immune evasion

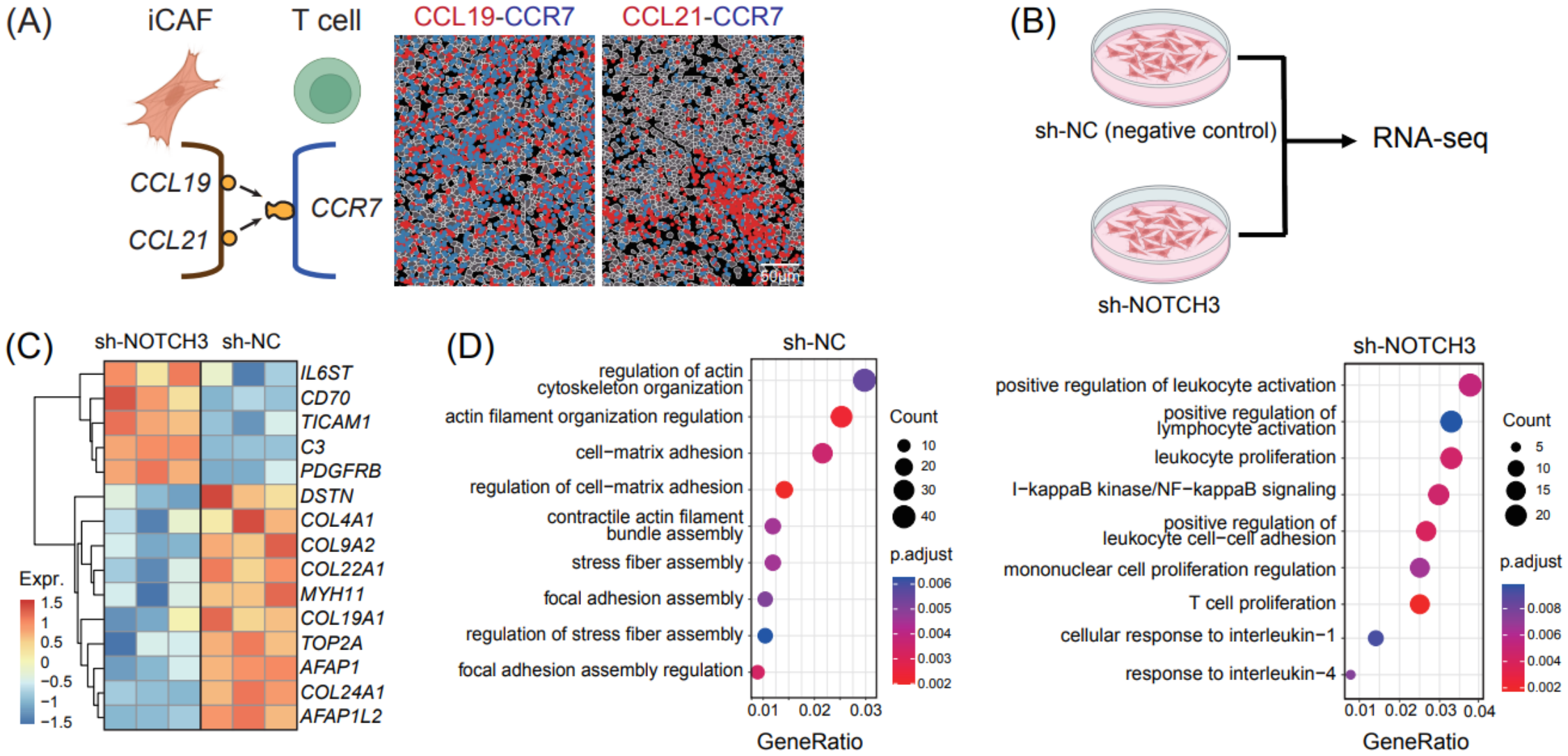

(A) Schematic spatial imaging plot of iCAF-T cells interaction mediated by CCL19/CCL21-CCR7. (B) Schematic diagram for *NOTCH3* knocking out (KO) experiment on human hepatic stellate cell line LX-2 cells for bulk RNA-seq. (C) Up-regulated and down-regulated genes between *NOTCH3*-KO and sh-NC LX-2 cell line. (D) Gene Ontology (GO) enrichment terms in *NOTCH3*-KO and sh-NC LX-2 cell line.

Co-culture shows DLL4-NOTCH3 axis drives collagen production

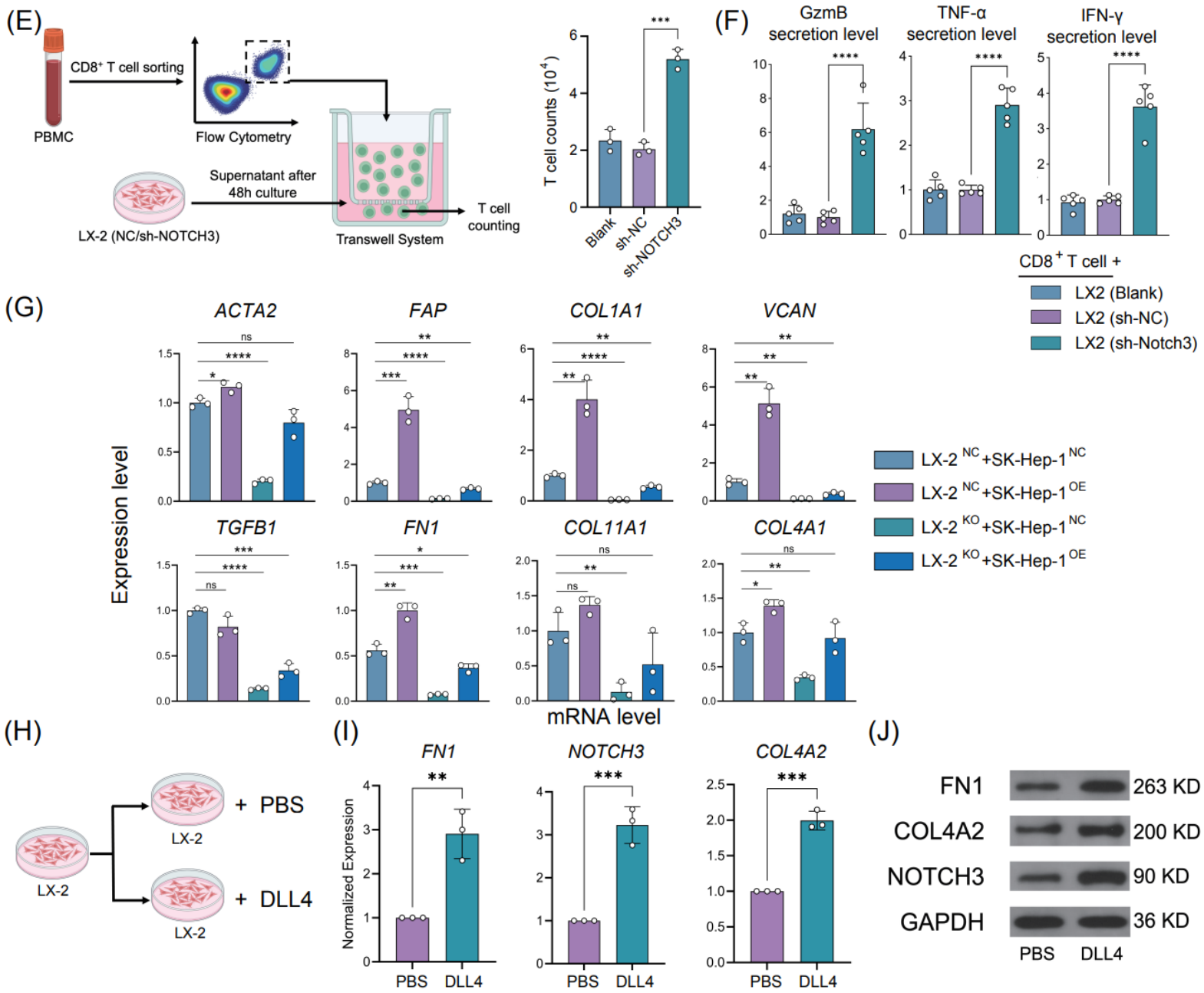

(E) Schematic diagram for the Transwell experiment and measurement of T cell migration and cytotoxicity. (F) Relative levels of GZMB, TNFα, and IFNg detected in the supernatant by ELISA. (G) qPCR results show the expression levels of genes related to fibrotic collagen polarization in different co-culture groups (SK-Hep-1 DLL4-overexpressing (OE) and SK-Hep-1 transfected with empty vector (NC); *NOTCH3*-knockout (KO) LX-2 fibroblasts and sh-NC LX-2 fibroblasts (NC). (H) Schematic diagram for LX-2 cells stimulated by DLL4. (I) qPCR analysis compares the mRNA levels of *FN1*, *NOTCH3*, and *COL4A2* between LX-2 cells with and without DLL4 stimulation. (J) Western blotting compares the protein level of FN1, NOTCH3, and COL4A2 between cells with and without DLL4 stimulation.

mCAF-macrophage spatial colocalization mediates immune evasion

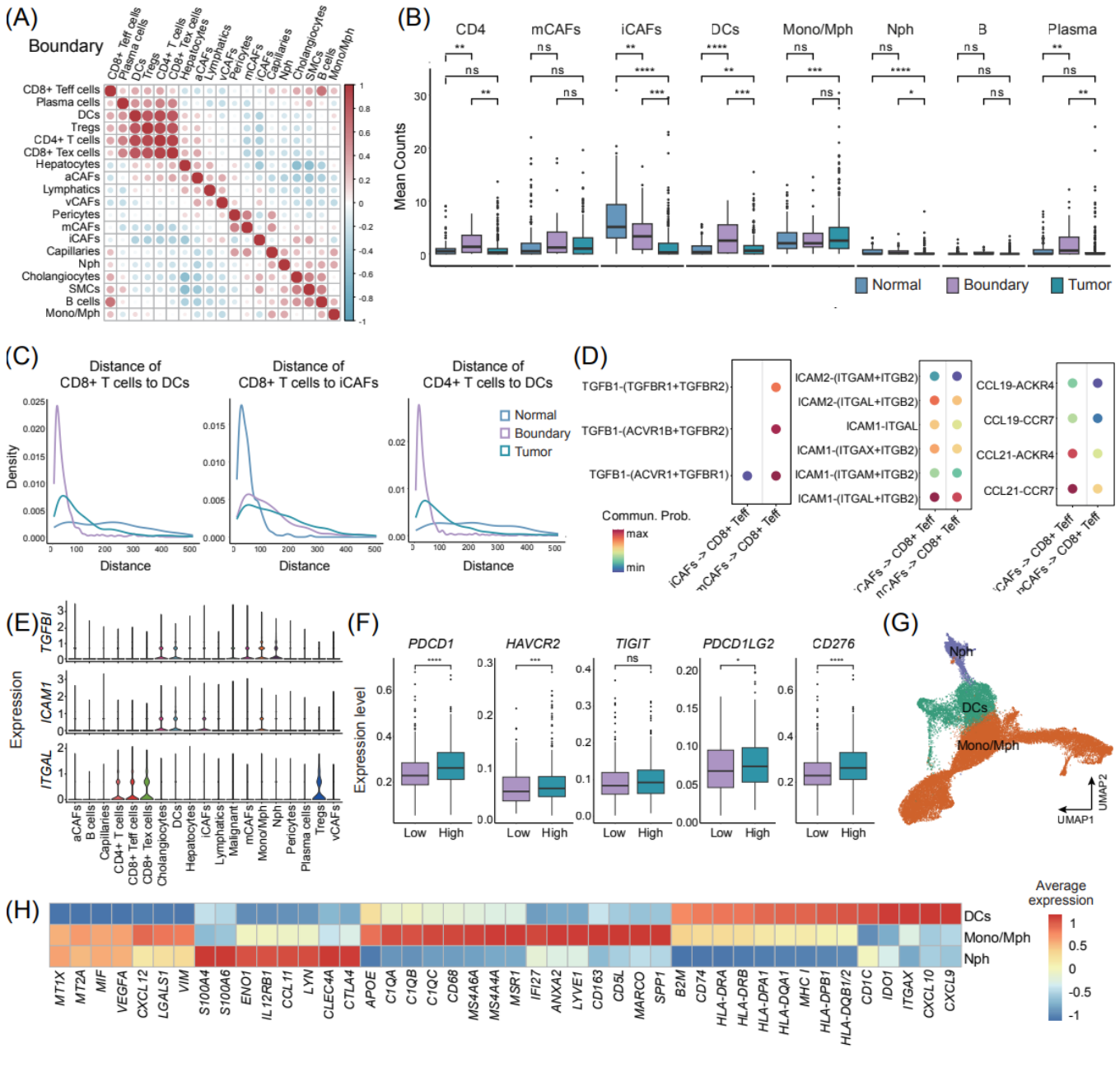

(A) Cell type frequency correlation analysis at the invasive tumor boundary shows a coordinated co-occurrence of CD4$^+$ T cells, DCs and CD8$^+$ T cells. (B) Mean counts of different cell types within spatial neighborhoods of 50 surrounding cells centered on CD8$^+$ T cells in Normal, Boundary, and Tumor regions. (C) Density plots showing the distance of CD8$^+$ T cells to DCs, iCAFs, and mCAFs in Normal, Boundary, and Tumor regions. (D) CellChat analysis between iCAFs/mCAFs and CD8$^+$ Teff. (E) Expression of *TGFBI*, *ICAM1*, and *ITGAL* across different cell types. (F) Box plots showing the expression levels of immune checkpoint genes (*PDCD1, HAVCR2, TIGIT, PDCD1LG2, CD276*) in mCAF-high and mCAF-low groups. (G) UMAP visualization for different myeloid subtypes. (H) Heatmap showing the expression levels of marker genes across different myeloid subtypes.

mCAF-macrophage spatial colocalization mediates immune evasion

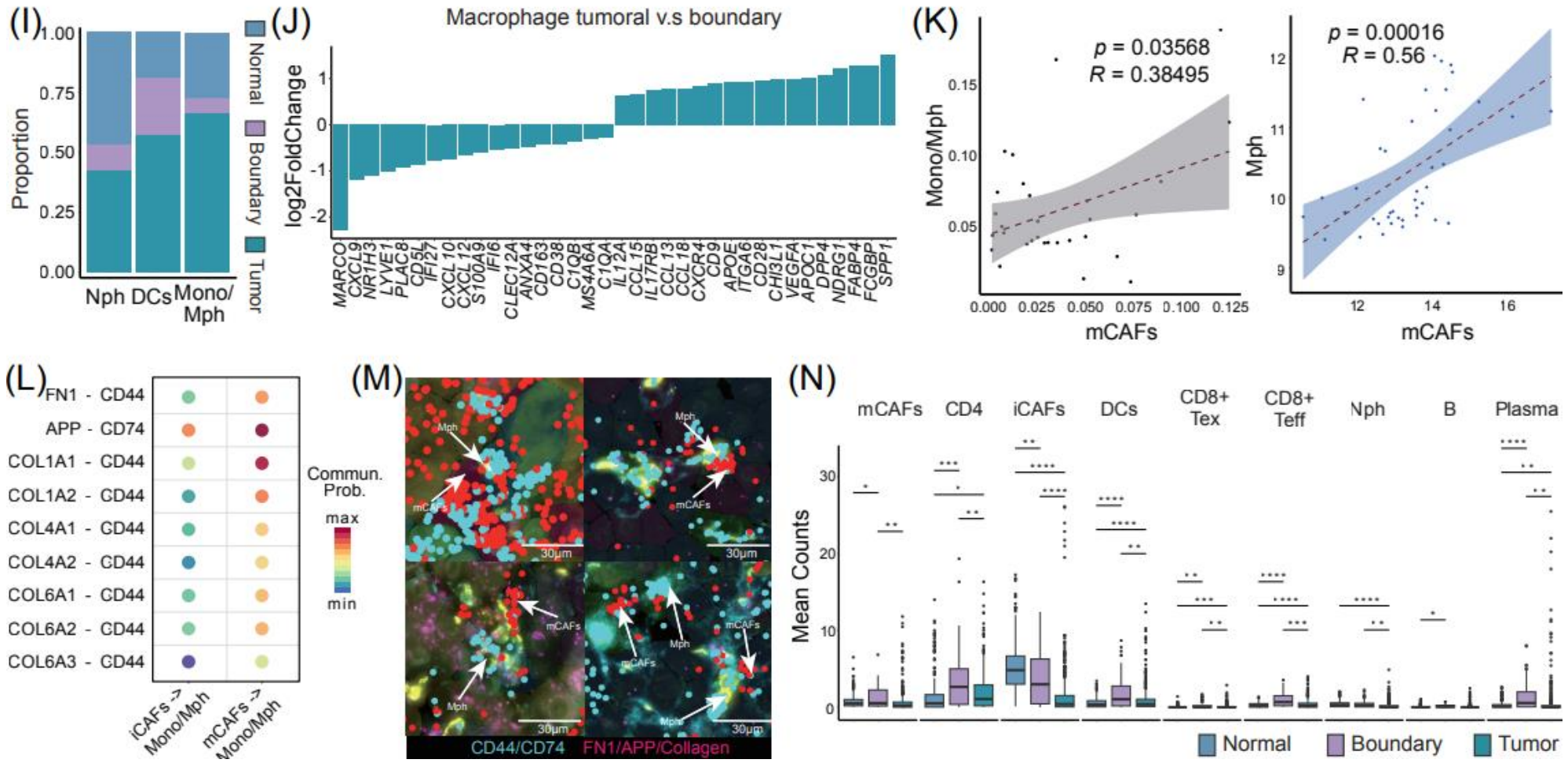

(I) The stacked barplot of different myeloid cell subtypes across Normal, Boundary, and Tumor regions in CosMx1000 data. (J) Ranked differentially expressed genes (DEGs) for macrophages between tumoral and boundary regions. (K) Scatter plot showing the correlation between mCAF and Mono/Mph proportions in the CosMx 1000 dataset (left). Scatter plot showing the correlation between mCAF and Mono/Mph signature scores in GeoMx 570 dataset (right). (L) CellChat analysis between iCAF/mCAF to Mph. (M) Spatial imaging plot showing the co-localization between mCAF and macrophages overlaid on the IF image, where mCAF associated ligand genes are labeled in red, Mph related receptor genes are labeled in Cyan. (N) Mean counts of different cell types within spatial neighborhoods of 50 surrounding cells centered on Mph in Normal, Boundary, and Tumor regions.

Orthotopic models show NOTCH inhibition sensitizes ICB therapy

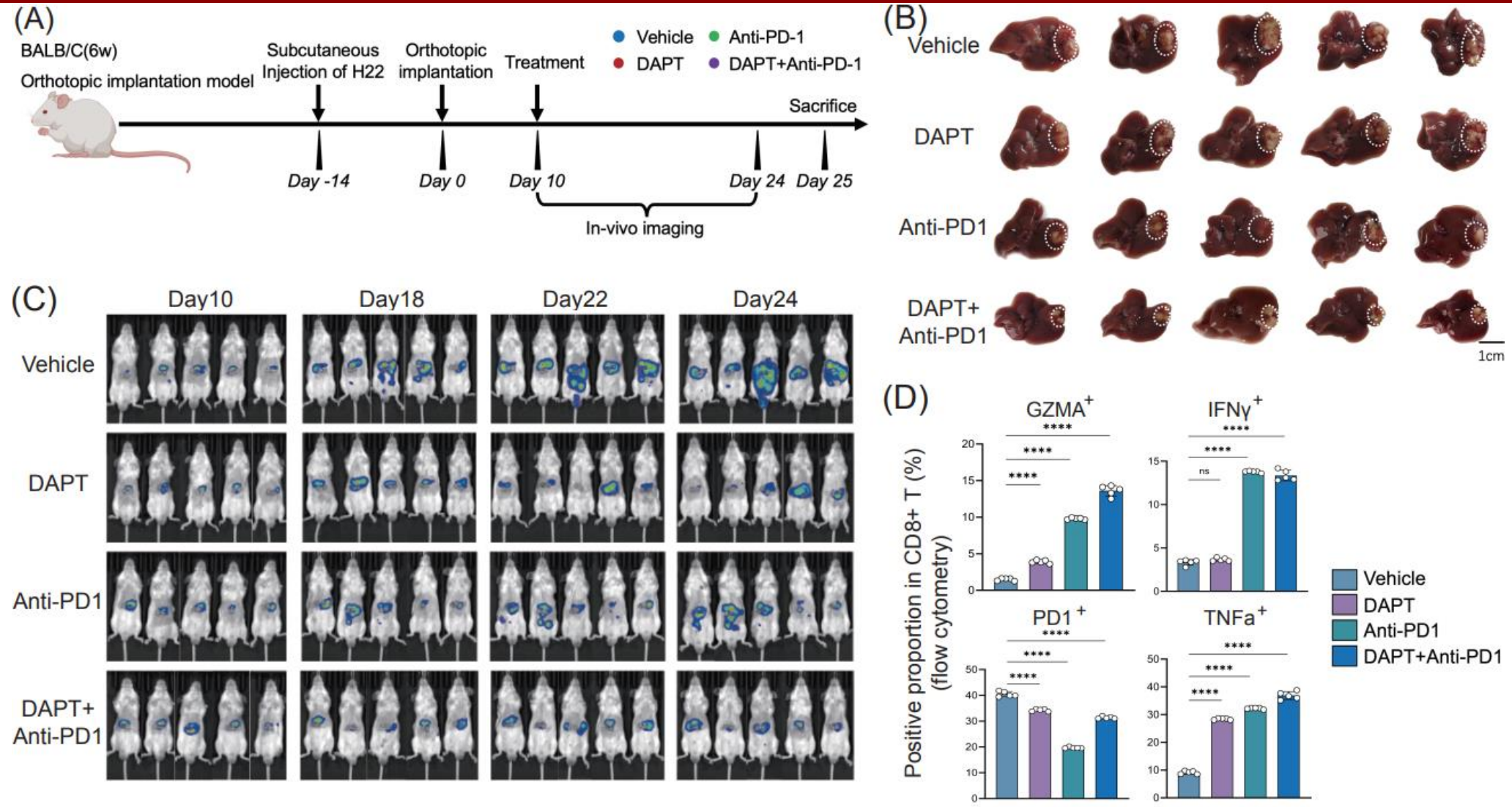

(A) Schematic diagram for establishing mouse liver cancer orthotopic implantation model, and applying treatment and in-vivo imaging on the model (DAPT: a small molecule NOTCH inhibitor). (B) Representative images of tumor size among different treatment groups using orthotopic implantation model. (C) In-vivo live imaging on different time points, comparing fluorescence signals among different treatment groups using orthotopic implantation model. (D) The proportion of $GZMA^+$, $IFN\gamma^+$, $PD1^+$, and $TNF\alpha^+$ cells in $CD8^+$ T cells, comparing among different treatment groups using orthotopic implantation model.

Spontaneous models show NOTCH inhibition sensitizes ICB therapy

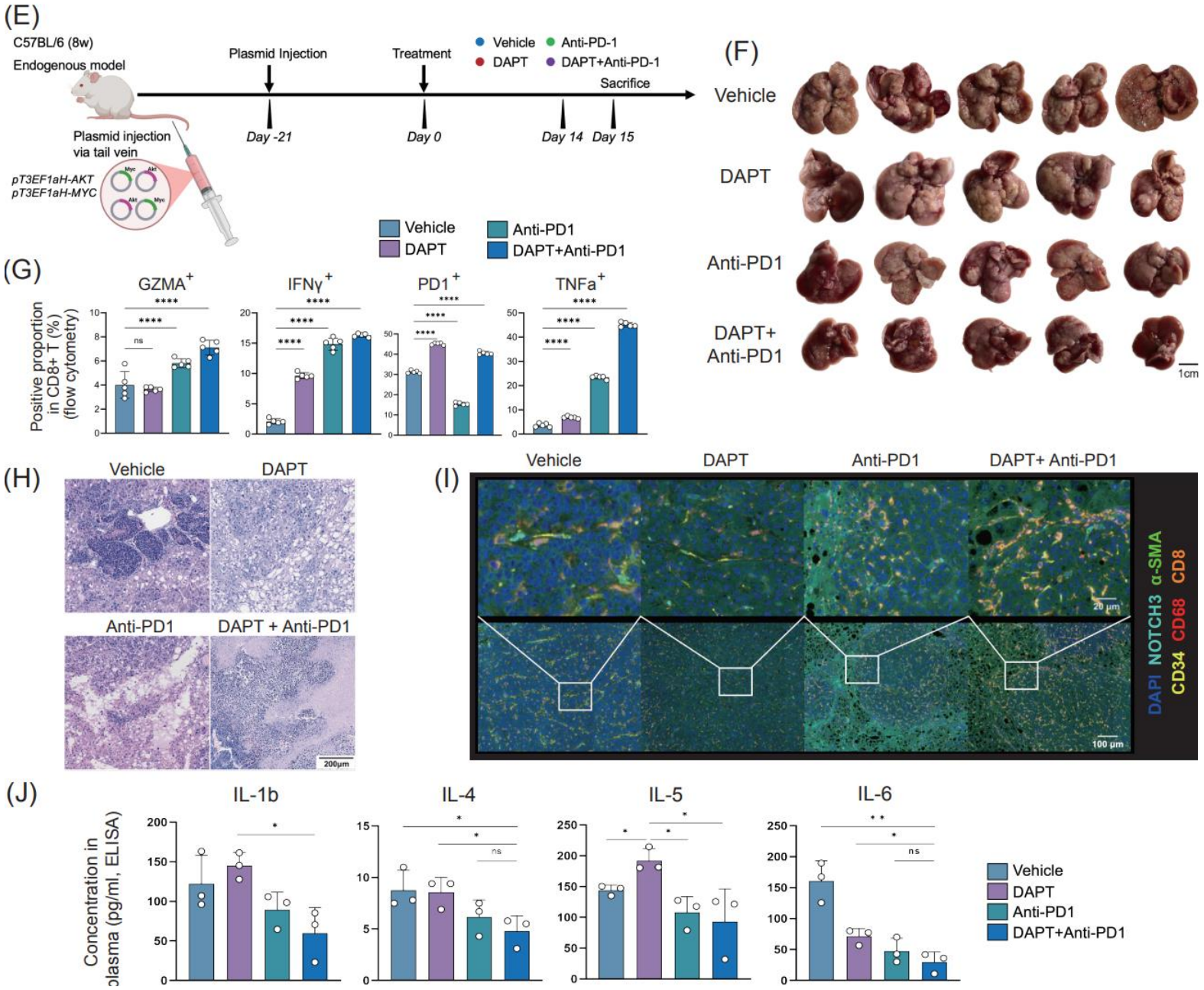

(E) Schematic diagram for establishing endogenous liver cancer mouse model and treatment. (F) Representative images of liver size among different treatment groups in the endogenous model. (G) The proportion of GZMA$^+$, IFNγ$^+$, PD1$^+$, and TNFα$^+$ cells in CD8$^+$ T cells from the endogenous model, comparing among different treatment groups in the endogenous model. (H, I) HE and multiplex immunohistochemical staining images of different treatment groups in endogenous model. (J) Concentration of IL-1b, IL-4, IL-5, and IL-6 in plasma of different treatment groups in the endogenous model.

Summary

- Multi-omics integration of HCC spatial data and pan-cancer ICB single-cell data systematically reveals a capillary-mCAF crosstalk network, proposing a new vessel-stroma framework driving immune exclusion.
- The DLL4-NOTCH3 signaling axis mediates mCAF polarization and matrix remodeling, constructing a "fibrotic barrier to T cell exclusion" mechanism and elucidating the key molecular basis of fibrosis-driven immune evasion.
- Functional experiments confirm that NOTCH blockade reverses mCAF differentiation, enhances T cell infiltration, and significantly improves ICB efficacy, establishing a complete evidence chain from mechanism to intervention.
- Targeting the NOTCH3 vessel-stroma axis offers a promising new strategy with clinical translation potential to overcome the immunotherapy bottleneck of "cold" HCC tumors.

Fansen Ji, Haochen Li, Qi Wang, Xiaojuan Wang, Jiawei Zhang, Ying Xiao, Huan Li, et al. 2026. Spatial Multi-Omics Identifies a NOTCH3-Mediated Capillary–mCAF Crosstalk Driving Immune Exclusion in Hepatocellular Carcinoma. ***iMeta*** 5: e70117. https://doi.org/10.1002/imt2.70117

iMeta: To be top journals in biology and medicine

WILEY

"***iMeta***" launched in 2022 by iMeta Science Society, impact factor (IF) **33.2**, ranking top 65/22400 in the world. It aims to publish innovative and high-quality papers with broad and diverse audiences. Its scope is similar to *Cell*. The average citation is > 40 in 2025, similar to *Nature* and *Science*. Its unique features include video abstract, bilingual publication, and social media with 600,000 followers. Indexed by **SCIE/ESI**, **PubMed**, **Google Scholar** etc.

"***iMetaOmics***" launched in 2024, indexed by **ESCI**, **PubMed**, **Google Scholar**, with a **target IF>15, and its scope is similar to** *Nature Communications*, *Science Advances*, *Advanced Science*, *Nucleic Acids Research*, etc.

"***iMetaMed***" launched in 2025, with a target IF>15, similar to *Med, Cell Reports Medicine, eBioMedicine, eClinicalMedicine* etc.

Society: http://www.imeta.science
Publisher: https://wileyonlinelibrary.com/journal/imeta
Submission: iMeta: https://wiley.atyponrex.com/journal/IMT2
iMetaOmics: https://wiley.atyponrex.com/journal/IMO2
iMetaMed: https://wiley.atyponrex.com/journal/IMM3

iMetaScience
iMetaScience

office@imeta.science
imetaomics@imeta.science

Promotion Video

Update
2026/3/30